

Slide 1

The slide features a background image of a stormy sea with a satellite in the sky. Overlaid on the image are several green and red lines representing atmospheric wave patterns. The text on the slide is as follows:

**Diagnostics 1**  
Mark Rodwell

Training Course on Predictability  
4 November 2024, ECMWF Reading

ECMWF European Centre for Medium-Range Weather Forecasts, Shinfield Park, Reading, RG2 9AT, UK © ECMWF November 4, 2024 mark.rodwell@ecmwf.int

Slide 2

The slide contains the following text:

**Outline**

- Tropical waves, teleconnections, and the propagation of errors
- Identifying the root-causes of forecast biases and assessing models

ECMWF European Centre for Medium-Range Weather Forecasts Mark Rodwell

This lecture focuses on the tropics. I will discuss tropical waves and teleconnections. These are important for predictability, but also act to propagate errors and uncertainties. How do we identify the root-causes of forecast errors in the face of such propagation and interaction?

Slide 3

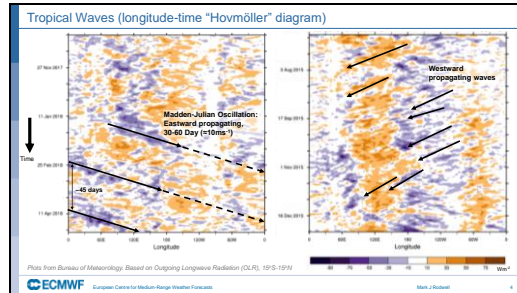
The slide contains the following text:

**Outline**

- Tropical waves, teleconnections, and the propagation of errors
- Identifying the root-causes of forecast biases and assessing models

ECMWF European Centre for Medium-Range Weather Forecasts Mark Rodwell

Slide 4



The Madden-Julian Oscillation (MJO) is thought to involve the interaction between (amongst other things) the convection and the large-scale dynamics. We can track the convection associated with the MJO by observing out-going long-wave radiation (OLR). This is because OLR is related to the temperature of the emitting surface. High, cold, convective cloud-tops are associated with negative anomalies in OLR.

The left 'Hovmöller diagram' indicates an MJO event propagating east. Observed MJO events generally propagate with a phase speed of about  $10\text{ms}^{-1}$ , making a single rotation of the equator in around 30 to 60 days. The forecast model also predicts OLR. Historically, models tend to produce too fast phase speeds for MJO-like features. This may be related to the faster phase speed of dry Kelvin waves (see later).

There are also waves that propagate to the west. The waves depicted in the right-hand panel are likely to be associated with the dynamics of equatorial Rossby waves (or mixed Rossby-gravity waves). The fact that they leave a signal on the OLR indicates one-way or two-way coupling with the moist physics.

Slide 5

Equatorial wave theory – the model

$\epsilon \ll \eta$

$\bar{g} = g \left( 1 - \frac{\rho_2}{\rho_1} \right)$  (Reduced gravity)

$\omega = \Omega \sin \theta$  (Coriolis mass)

$c_g^2 = g \frac{\Delta \rho_2}{\rho_1 \Delta \rho_1} = g \bar{g}$ ,  $c_g \sim 20$  to  $80 \text{ m s}^{-1}$

$c_g$  is the propagation speed of a barotropic gravity wave in a single layer of depth  $H_1$ .

**Momentum:**

$$\frac{\partial u}{\partial t} - \beta y v + g' \frac{\partial \eta}{\partial x} = 0$$

$$\frac{\partial v}{\partial t} + \beta y u + g' \frac{\partial \eta}{\partial y} = 0 \quad (1)$$

**Continuity:**

$$\frac{\partial \eta}{\partial t} - c_g^2 \left( \frac{\partial u}{\partial x} + \frac{\partial v}{\partial y} \right) = 0 \quad (2)$$

**Solving for  $v$ :**

$$\frac{\partial}{\partial t} \left( \frac{\partial v}{\partial t} + \beta^2 y^2 v - c_g^2 \left( \frac{\partial^2 v}{\partial x^2} + \frac{\partial^2 v}{\partial y^2} \right) \right) - c_g^2 \beta \frac{\partial v}{\partial x} = 0 \quad (3)$$

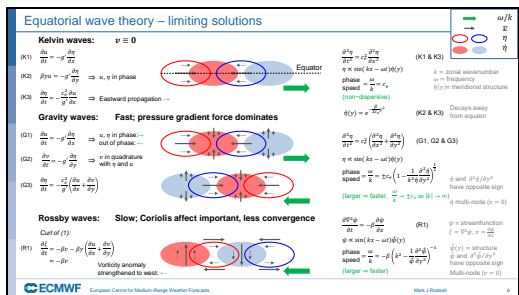
Use of the shallow water equations on the  $\beta$ -plane ( $f = \beta y$ ) for understanding tropical atmospheric waves. Note: No coupling with convection in this model

ECMWF European Centre for Medium-Range Weather Forecasts

Sorry this slide is quite detailed, and the next ones are also quite mathematical! I wanted to make sure that I included a fairly rigorous mathematical explanation of tropical variability for those who are particularly interested. Below is a more descriptive explanation. The notes below the next slide contain more mathematical details. The simplest model for the tropics must include two levels. This is because, for example, deep convection plays a major role in the tropical circulation (monsoons, MJO etc). Deep convection involves low-level convergence and upper-level divergence and hence the need for at least two levels. Here convective heating is considered as a forcing, and we investigate the response to this forcing in terms of a ‘package’ of free (dry) waves. These waves can propagate and thus lead to communication between different regions of the tropics. In general, waves need to interact with a ‘force’. Gravity is one such force. The horizontal pressure gradient at the interface between two layers of different density (indicated on the figure) is proportional to a ‘reduced gravity’  $g'$  which takes account of these differing densities. Internal gravity waves are associated with this effect. Another ‘force’ is associated with the ‘Coriolis force’ (which exists because we are measuring winds relative to our rotating planet) and is perpendicular to the flow – indicated on the figure. This enters tropical wave theory through the ‘ $\beta$ -effect’ and leads to the existence of Rossby waves. The winds associated with a

positive (negative) vorticity anomaly transport or 'advect' positive (negative) planetary vorticity to the west of the original anomaly and thus Rossby waves have a westward phase speed. Mixed Rossby-gravity waves are associated with both processes. A further class of waves are the Kelvin waves. These waves are in geostrophic balance with the meridional pressure gradient. Using this fact, it is relatively easy to see that Kelvin waves must propagate to the east.

Slide 6



We can get an idea of the wave solutions by looking at limiting cases. The simplest set of solutions is found by inserting  $v \equiv 0$  in the equations on the previous slide - this is clearly a solution to (3). When we do this, we get the **Kelvin waves**. Notice that the zonal wind difference between the two levels,  $u$ , is in geostrophic balance with the pressure gradient (K2). The red and blue open ellipses represent a hypothetical wave in  $\eta$ . By examining equation (K2), we see that  $u$  is in phase with  $\eta$ , and that the tendency (the red and blue shaded ellipses) acts to move the whole wave to the east (K3). We can look for mathematical solutions (like in the equations on the right), with a sine wave in the zonal direction multiplied by a structure function in the meridional direction. Notice that the phase speed of the sine wave is given by  $\partial x / \partial t = \omega / k = c$ , so that phase speed  $= \partial x / \partial t = c = \omega / k$ . For the Kelvin waves, combining (K1) and (K3) gives us  $\partial^2 \eta / \partial t^2 = c^2 \partial^2 \eta / \partial x^2$  which is a constant. Whatever the spatial scale of the wave, it always travels at the same speed. This means that Kelvin waves are non-dispersive - if we had two or more Kelvin waves super-imposed, the pattern of the wave packet would not change as it moves east. Combining (K2) and (K3), we find that the meridional structure function is simply an exponential that decays away from the equator.

There are a class of fast-moving waves for which the Coriolis effect is not important. Dropping the terms involving  $\beta$  in the equations on the previous slide, we get the **Gravity wave** solutions. Since  $u$  reaches a maximum (or minimum) at a given location when  $\partial u / \partial t = 0$ , (G1) shows that this occurs with  $\partial \eta / \partial x = 0$ , and hence  $u$  has either the same phase, or opposite phase to  $\eta$ . (G1) shows that, when they have the same (opposite) phase, the wave propagates to the

east (west). I have drawn both possibilities. (G2) shows that meridional wind  $v$  is maximum or minimum when  $\partial\eta/\partial y = 0$ , and so is in quadrature with  $\eta$  and  $u$ : we get regions of horizontal convergence and divergence. For these waves, the meridional structure function can have several nodes, and the waves can be repeated several times across the tropical channel (see the wave-spotting exercise). The absolute value of the phase speed is greater than  $c_g$  (because  $\partial\eta/\partial y$  and  $\partial^2\eta/\partial y^2$  have opposite sign) and tends to  $c_g$  as  $k$  increases (smaller  $k \Rightarrow$  larger wave  $\Rightarrow$  faster).

Another class of waves is slow-moving, and the Coriolis term can't be ignored. These are the **Rossby waves**. In this case, the flow is closer to geostrophic balance and thus tends to flow around the height anomalies. Hence it is useful to think in terms of vorticity and thus take the curl of (1). Neglecting the convergence term (the "Ballerina effect" – see next lecture), we see that the local vorticity tendency is related to the meridional advection of planetary vorticity  $\beta v$  (R1). If we have a positive (negative) vorticity circulation, then the meridional winds to the west of this circulation will advect-in higher (lower) values of planetary vorticity and so the wave will always have a westward phase speed  $\omega/k < 0$ . Notice that the larger waves (smaller  $k$ ) will propagate westward fastest (larger wave  $\Rightarrow$  faster).

There is also an intermediate class of waves (so not apparent in these limiting solutions) that have the characteristics of both Gravity and Rossby waves (in varying degrees). The ones that have eastward phase speed are more like Gravity waves whereas the ones with westward phase speed are more like Rossby waves.

The next slide gives a more complete mathematical account of all the waves (for the interested reader).

Free Equatorial Waves		Not discussed in lecture
$V=0$ :	$u = u_0 e^{i(kx - \omega t)}$	East propagating Kelvin Wave <ul style="list-style-type: none"> <li>Non-dispersive</li> <li>In geostrophic balance</li> </ul>
$V \neq 0$ :	$v = \tilde{v}(y) e^{i(kx - \omega t)}$	Substitute into equation for $v$
Structures (Meridional structures are solutions to Schrodinger's simple harmonic oscillator)	$\tilde{v}(y) = \begin{bmatrix} 1 \\ 2y \\ 4y^2 - 1 \\ 8y^3 - 12y \\ \vdots \\ H_n(y) \end{bmatrix} e^{-y^2/2}$	Hermite Polynomials: $H_n(y)$ <ul style="list-style-type: none"> <li>Each successive polynomial (<math>n=0, 1, 2, \dots</math>) has one more node</li> <li>Modes alternate asymmetric / symmetric about equator</li> </ul>
Dispersion (How phase speed is related to spatial scale)	$\left(\frac{\omega}{c_0} + k^2 - \frac{\beta k}{\omega}\right) = (2n+1) \frac{\beta}{c_0}$ ( $n = 0, 1, 2, \dots$ )	For $n \neq 0$ : 3 values of $\omega$ for each $k$ <ul style="list-style-type: none"> <li>West propagating Rossby Wave</li> <li>E &amp; W propagating Gravity Wave</li> </ul> For $n=0$ : 2 values of $\omega$ for each $k$ <ul style="list-style-type: none"> <li>E &amp; W prop. Mixed Rossby-Gravity</li> </ul>

Note:  $y$  has been non-dimensionalised by the factor  $(2/\beta c_0)^{1/2}$ .  
 In dispersion relation, gravity waves mixed associated with first two terms on the left. Rossby waves with last two terms on the right. Mixed Rossby-gravity waves with all three terms.

One immediate solution to equation (3) two slides ago is  $v \equiv 0$ . Inserting  $v \equiv 0$  into equations (1) and (2) and looking for solutions which are separable in  $x$  and  $y$  and decay as  $y \rightarrow \pm\infty$ , one finds waves of the form given for  $v=0$  above. Here,  $k$  is the zonal wavenumber of the wave (the number of waves around a latitude circle) and this can take any positive value. This class of waves is known as the equatorial Kelvin waves. Whatever the value of  $k$ , the wave propagates eastward with a speed  $\beta/c_0$ . Hence the Kelvin waves are 'non-dispersive' with waves of different spatial scale all having the same eastward phase-speed. For reasonable values of  $\beta$ ,  $H_0$ ,  $H_1$ ,  $H_2$ ,  $\rho$  and  $\rho_0$ , the speed  $\beta/c_0$  may be between 20 and 80  $\text{ms}^{-1}$ .

If  $v \neq 0$ , then one can look for separable solutions to equation (3) which, as before, decay as  $y \rightarrow \pm\infty$ .

Substituting

$v = \tilde{v}(y) e^{i(kx - \omega t)}$  into (3), one obtains the equation for the meridional structure,  $\tilde{v}(y)$ , of the solutions:

$$\left(\frac{\omega}{c_0} + k^2 - \frac{\beta k}{\omega}\right) \tilde{v} = (2n+1) \frac{\beta}{c_0} \tilde{v} \quad (N1)$$

Equation (N1) is Schrödinger's simple harmonic oscillator with the meridional structure  $\tilde{v}(y)$  being the Eigenvector, and the multiplier of  $\tilde{v}(y)$  on the right-hand-side being the corresponding Eigenvalue. It can be shown by substitution that a solution (the simplest) is

$$\tilde{v}(y) = e^{-y^2/2} \quad , \quad \left(\frac{\omega}{c_0} + k^2 - \frac{\beta k}{\omega}\right) = \beta$$

$$k\omega = \beta c e^{-\beta y} \quad \omega = \lambda^2 \theta \quad (N2)$$

where  $v_{\theta}$  is an Eigenvector and  $\lambda^2$  its corresponding Eigenvalue. In this solution, the meridional wind is maximum on the equator and decreases in strength as the latitude increases. The other solutions to equation (N1) can be obtained by 'induction' from this first solution. To demonstrate this, note that the differential operator on the left-hand-side of (N1) can be written in two ways:

$$\beta^2 \frac{\partial^2 \theta}{\partial y^2} - \frac{\partial^2 \theta}{\partial y^2} = \beta^2 \frac{\partial^2 \theta}{\partial y^2} - \frac{\partial^2 \theta}{\partial y^2} + \frac{\partial^2 \theta}{\partial y^2} \quad (N3)$$

$$= \beta^2 \frac{\partial^2 \theta}{\partial y^2} + \frac{\partial^2 \theta}{\partial y^2} - \beta^2 \frac{\partial^2 \theta}{\partial y^2} - \frac{\partial^2 \theta}{\partial y^2} \quad (N4)$$

Using (N3) and (N4), it is straightforward to show that, if  $v_{\theta n}, \lambda^2 n$  is an Eigenvector / Eigenvalue solution then so is

$$v_{\theta n+1} = \beta^2 \frac{\partial^2 v_{\theta n}}{\partial y^2} - \frac{\partial^2 v_{\theta n}}{\partial y^2}, \quad \lambda^2 n+1 = \lambda^2 n + 2\beta^2 c e^{-\beta y}.$$

Hence the series of solutions:

$$v_{\theta n} = \beta^2 \frac{\partial^2 v_{\theta n-1}}{\partial y^2} - \frac{\partial^2 v_{\theta n-1}}{\partial y^2} - \beta^2 c e^{-\beta y} \frac{y^{2n}}{2^n}, \quad \lambda^2 n = 2n + 1 \beta^2 c e^{-\beta y}$$

for  $n=1,2,\dots$

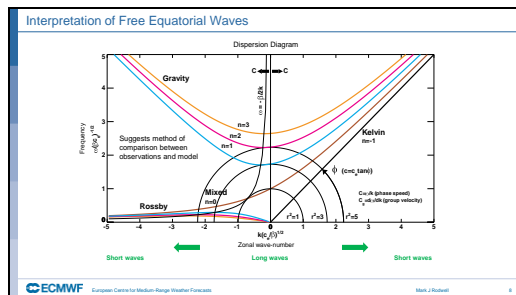
The Eigenvectors,  $v_{\theta n}$ , are the 'Hermite polynomials' (multiplied by  $e^{-\beta y} - \beta^2 c e^{-\beta y} y^2 / 2$ ). The first few are shown in the slide above. Each polynomial has one more node (latitudes where  $v_{\theta n}$  is zero)

than the previous polynomial and successive polynomials alternate between being asymmetric and symmetric about the equator (for symmetric modes

$$\frac{\partial v}{\partial n} - y = - \frac{\partial v}{\partial n} - y$$

The Eigenvalues define the ‘dispersion relation’ as shown in the slide. This will be illustrated on the next slide.

Slide 8

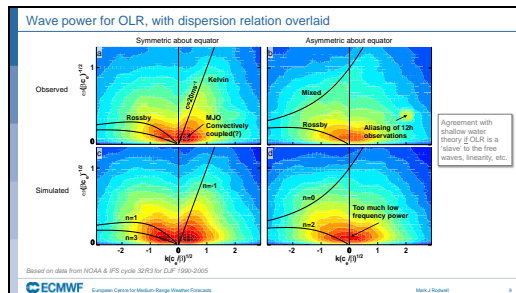


The dispersion relation can be used to plot a ‘dispersion diagram’. This diagram shows how wave-number  $k$  and frequency  $\omega$  are related for each class of waves. Note that  $k = \frac{2\pi}{\lambda}$  where  $\lambda$  is the wavelength in the zonal direction. Similarly  $\omega = \frac{2\pi}{\tau}$  where  $\tau$  is the period of the oscillation at any given point. Waves (equatorial wave solutions) exist for all points on the coloured curves. The value of  $n$  for each curve relates to the meridional structure of the wave – it is the number of latitudes where the meridional wind is zero. The zonal phase-speed of each wave is  $c = \frac{\omega}{k}$  (for the aspect ratio of the diagram above, this can also be written as  $c = c_0 \tan \phi$ ). The top set of coloured curves relate to the gravity waves. They have relatively high frequency and fast phase speeds. These phase speeds can be both eastward and westward. The lower curves relate to the Rossby waves. These have smaller frequencies and slower phase speeds which are always westward (relative to any background



flow). The brown curve relates to the mixed Rossby-gravity waves. There is only one meridional structure for these waves but they can have any zonal wavelength. The black diagonal line relates to the Kelvin waves. For these waves there is also only one meridional structure and they can have any zonal wavelength. Whatever the wavelength however, the phase-speed of the Kelvin waves is always the same ( $c = \sqrt{gH}$  eastward). Since the phase-speed is always the same, these waves are non-dispersive (waves of different wavelength do not change their phase relationship with each other – as we will see in the animation).

Slide 9

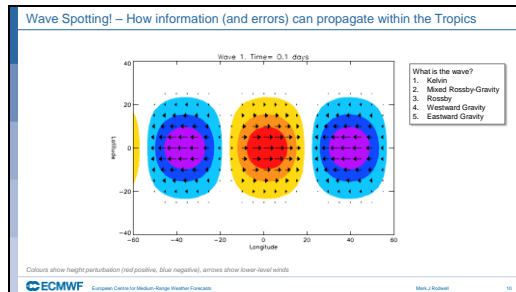


Using out-going long-wave radiation (as in the Hovmöller example) it is possible to isolate the wave power for each wavenumber and frequency. This has been done in panel (a) for the observed symmetric waves and overlaid with the dispersion diagram. The agreement is quite amazing (to me at least!) . The higher wave power can be seen for both the Rossby and Kelvin waves. The observations are not frequent enough to allow us to calculate the power in the gravity waves. The region of high power at small positive wavenumber and small frequency relates to the Madden-Julian Oscillation (MJO). The MJO is not on any of the curves and this demonstrates that the MJO is not adequately represented by the Shallow water model. A likely reason could be that the MJO involves coupling with the physics (convection,

radiation *etc*). A reasonable agreement can also be seen between the theoretical symmetric waves and those found in the ECMWF model cycle 32R3, here run at resolution T<sub>L</sub>159L91 (panel c). The ECMWF model cycle 32R3 had a major change to its convection. The entrainment of moisture into a convective plume used to be partly due to turbulent processes and partly related to the large-scale convergence. At cycle 32R3, the explicit connection to the large-scale convergence was removed. This had many beneficial impacts on forecast scores and on synoptic activity. Unfortunately, it also strongly increased low-frequency, planetary activity. This over-estimation of low-frequency activity is clearly visible in panel (c) (when compared to panel a). The entrainment change may well have had a major impact on wave-convective coupling. For the asymmetric waves, the mixed Rossby-gravity waves are apparent in the observed OLR data (panel b). The large power near (non-dimensionalised) wavenumber 2 is spurious and due to satellite sampling that involves 14 passes around the length of the equator. The model (panel d) tends to capture the asymmetric Rossby waves but doesn't appear to capture the distinct set of mixed Rossby-gravity waves seen in the observations.

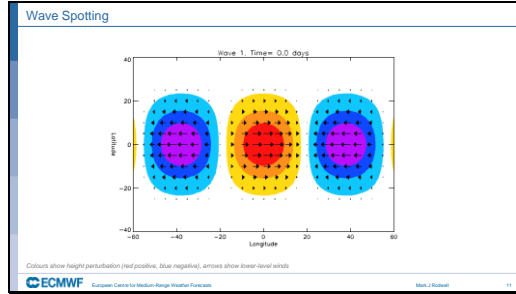
More generally, the ability of a model to accurately represent the spatio-temporal variability of the atmosphere is of fundamental importance in forecasting, and such diagnostics are, therefore, very important.

Slide 10

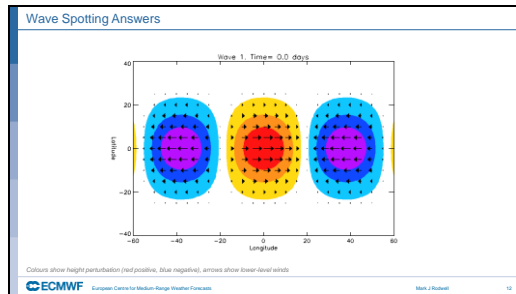


There are ‘bird spotters’ and ‘train spotters’ and so why not ‘wave spotters’? This is an animation of equatorial waves as deduced from the shallow water model. I made this partly so that I could get a better feeling for these waves and how they can communication information throughout the tropics. Here, the animation is used as a light-hearted ‘test’ to see if we can spot the different waves from their particular characteristics (phase-speed, meridional structure, whether meridional wind is zero or not, *etc*). Use the table in the next slide to fill-in your answers.

Slide 11



Slide 12



Slide 13

Wave spotting: Your Answers

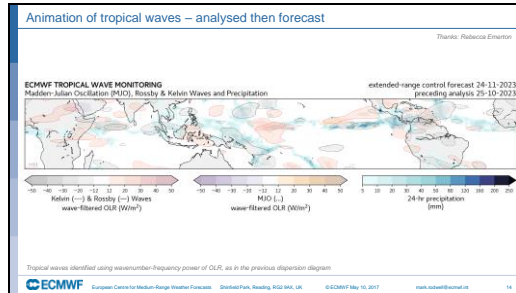
Wave	Kelvin	Mixed Rossby-Gravity	Rossby	Eastward Gravity	Westward Gravity
1					
2					
3					
4					
5					
6					
7					
8					
9					
10					
11					
12					

ECMWF European Centre for Medium-Range Weather Forecasts

Mark Roberts

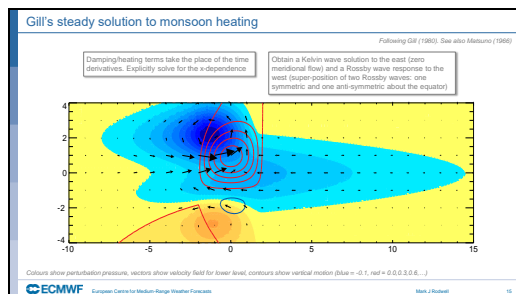
13

Slide 14



This animation depicts Kelvin and Rossby waves, and the MJO, deduced using the OLR dispersion diagram. Also shown is the total precipitation. Such animations are produced routinely at ECMWF, with the first part of the animation being based on past analyses and the second part on the forecast. We can see the various waves propagating eastward and westward, and sometimes associated with extreme rainfall events.

Slide 15

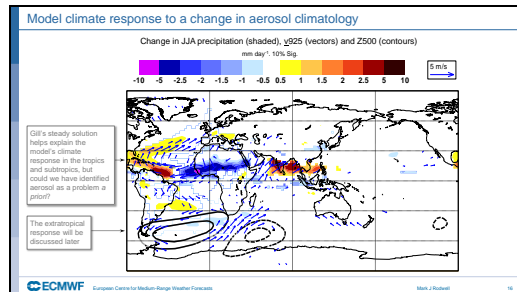


Gill (1980) solved the equatorial wave equation as a solution to fixed heating and a damping term. The above figure is his 'monsoon' result. The red contours show the centre of off-equatorial monsoon heating. The flow to the east is a Kelvin wave. The flow to the west of the heating is the sum of two Rossby waves – in this appear to be the seeds for the so-called Monsoon-Desert mechanism. If we simulate tropical convection wrongly it is clear that, quite quickly, the large-scale flow will develop errors, and these errors will interact back with the convection and other model process.

Because of these interactions, when examining an erroneous seasonal-mean model climate, it will be very difficult to isolate the root cause of the error. Of course, interactions take place all the time (not just associated with tropical waves) and possible approach to avoiding these complications is to look at errors very early on in the forecast, before such interactions have taken place. This is the main justification for using the

initial tendencies approach to be discussed shortly. Firstly, however, we look at a real example of where such waves are evident in the model climate.

Slide 16



Many of the features of Gill's steady solution to monsoon heating are seen in the IFS model climate response to a change in aerosol (all with the opposite sign). For example, we see a weakening of the North African monsoon, together with an anticyclonic Rossby-wave response to its west and an upwelling Kelvin-wave to its east – which triggers strongly enhanced precipitation. All these changes represented improvements to the model climate. However, if our purpose in Diagnostics is to identify the root-cause of forecast deficiencies, it might have been quite difficult to identify, *a priori*, aerosol as a key problem for the model climate. More generally, the dispersion (and interaction) of waves complicates a simple local diagnosis of model error.

In addition to helping explain such large-scale responses, equatorial waves (and waves in general) can provide predictability by linking weather in one region back to more slowly-varying 'drivers' in another region.

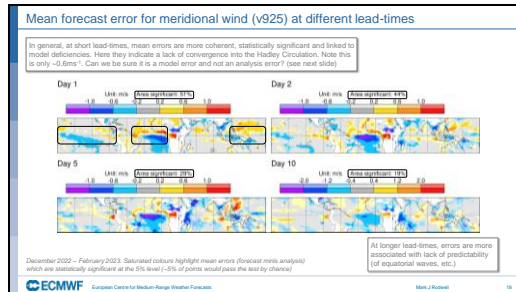
Slide 17

Outline

- Tropical waves, teleconnections, and the propagation of errors
- Identifying the root-causes of forecast errors and assessing models

ECMWF European Centre for Medium-Range Weather Forecasts Slide 17/20

Slide 18



The figure shows 925 hPa meridional wind errors averaged over all operational 0 and 12 UTC forecasts made at ECMWF for the season December–February 2022/23. The four plots show these mean errors for the forecast lead-times of 1, 2, 5, and 10 days, respectively. At Day 1 there appears to be a widespread and statistically significant lack of convergence into the Inter-Tropical Convergence Zone (ITCZ). 5% significance is indicated by the use of the more saturated colours, while insignificance is indicated by the use of less saturated colours. (5%

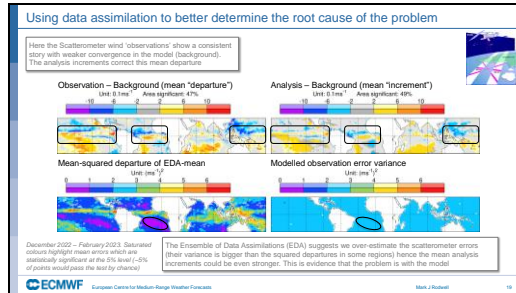
significance means that ~5% of the area might be expected to pass the test by chance alone. Since the area-significant is actually 51%, the signal is highly field-significant.

Through Days 2, 5, and 10 the pattern of tropical error seen at day 1 is replaced by a more complex pattern, and the area which is significant at the 5% level decreases.

An interpretation of these results is that, as lead-time increases, interactions, teleconnections and loss of predictability have confused a simple investigation of the root causes for the mean forecast error. Statistical significance actually increases as the lead-time decreases. Taken to the ultimate extreme, one might expect that the best lead-time to use when searching for physical parametrization deficiencies would be at timestep 1 of the forecast! (see, *e.g.*, Klinker and Sardeshmukh; 1992). In fact, just using timestep 1 introduces other problems associated with sampling the diurnal cycle so here the focus will be on the first 12 hours. These are, in fact, the timesteps within the data assimilation window and much of our focus will be on the data assimilation system.



Slide 19

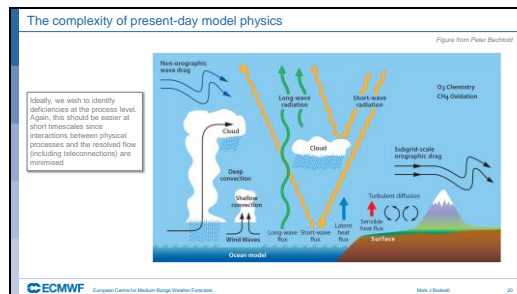


Sometimes there are observations used within the data assimilation system which appear to directly highlight the same mean “errors”. For example, scatterometer data are used to infer surface winds from satellite-observed backscatter over the oceans, and these winds are assimilated. In the top panels, the mean background departures (also known as first-guess departures) for meridional winds highlight reduced tropical convergence in the model background compared to the observations. The mean analysis increments act to increase the convergence in the new analysis relative to the background. The actual magnitude of the mean departures and increments is quite small, and we might ask whether the observations are accurate-enough to be able to say that the problem lies with the model? We can attempt to answer this question by looking at a variance budget of the Ensemble of Data Assimilations (EDA) in the bottom panels. The full budget decomposes the mean-squared departure of the EDA-mean background into a background variance term (also known as “spread”) and an observation error variance term (along with squared bias and variance deficiency terms). This budget is much like the well-known “error-spread” relationship but taking observation uncertainty into account. Here it is enough to just show the mean-squared departures and the modelled observation error variances. In some regions, such as in the subtropical anticyclone regions, the observation error variances are actually larger than the squared

departures. This is strong evidence that we over-estimate these observation errors. Since these observation error estimates apply globally in this case, the implication is that, if anything, the analysed mean tropical convergence does not draw close-enough to the observed values, and thus that we can trust the sign of the mean increment. The conclusion is that the weaker convergence in the background forecast is a sign of a model problem.

Note that it could be too simplistic to conclude that we should decrease our modelled values of observation error variances immediately, as this could lead to other problems (for example “tram-lines” over the analysis showing the location of the satellite tracks in any given assimilation window!)

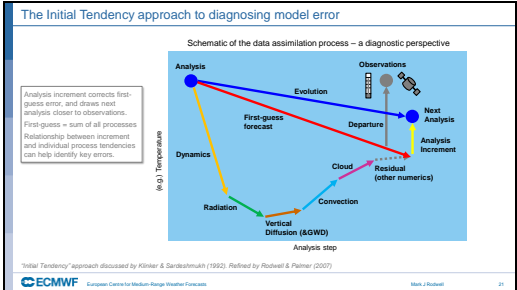
Slide 20



Much model development is driven by a ‘bottom-up’ desire to improve the representation of underlying physical processes. Such development is undertaken at ECMWF by researchers with responsibility for a given physical process. They use, for example, single-column models driven by fixed boundary conditions. However, we also need to evaluate the impact of such changes in the full forecast system, and to identify residual issues. This task is one of the functions of Diagnostics. With the increasing complexity (and accuracy) of present-day models, which include increasing numbers of physical and micro-physical processes, with considerable

scope for interaction between themselves and with the resolved flow, this task is always challenging! Focusing on short timescales should help here as such interactions are minimised and the processes are being applied to our best estimate of the true state (*i.e.* the analysis) - before model “drift” for example.

Slide 21



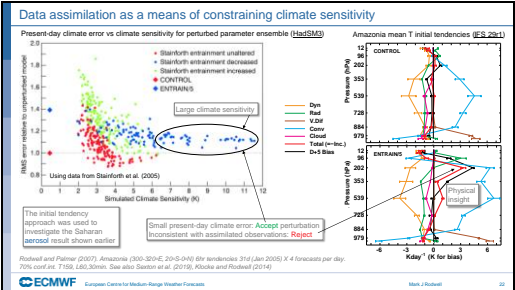
One approach to over-coming the issues of predictability and model complexity is to look very early-on in the forecast. Indeed, to look at the forecast model within the data assimilation system itself. With every data assimilation cycle, the model is effectively assessed against millions of new observations. I will discuss such an approach in this talk.

The data assimilation system acts to draw the analysis away from the “first-guess” (or “background” forecast) and closer to the observations in a way that is consistent with estimated observation and first-guess errors. The difference between the final analysis and the first-guess is known as the ‘analysis increment’. This can be viewed as a correction to the first-guess forecast. What I term the ‘analysed evolution’ of the flow is the difference between successive analyses. Note that the first-guess forecast is simply the sum of the tendencies from the dynamics and the physical processes (and any other numerics) represented within the model. In the schematic, the impact of

each process has been accumulated over all model timesteps within the data assimilation window - so that we can see the accumulated effect of each process. If the forecast model is perfect and the observations unbiased then, when averaged over many data assimilation cycles, the mean analysis increment should be zero (or at least very small). In such a situation, the contributions from all the processes should be almost in balance (since the analysed evolution is also small when averaged over many cycles). If the mean analysis increment is not zero, then this indicates that the model processes are not correctly in balance and that some aspect(s) of the model contain errors. (This assumes that the observations are unbiased, which is a reasonable assumption since the 'variational bias correction scheme' acts to remove large-scale systematic departures from the first-guess). How might such an imbalance arise? The concept of 'radiative-convective' equilibrium embodies the idea that radiative processes act to destabilise the atmosphere (heat the surface and cool the mid-to-upper troposphere) and the convection induced by this destabilisation acts to restore balance by cooling the surface and heating the mid-to-upper troposphere. With this idealised concept in mind, either a convection scheme that is too weak (given the observed temperature and humidity profiles) or a radiation scheme that is too strong (given the observed conditions – humidity *etc.*; as embodied by the analysis) would lead to a systematic initial *net* cooling of the mid-troposphere. Assuming there are relevant observations present, this

cooling would be corrected with positive analysis increments. With the mean initial tendencies (or analysis increments), we therefore have a diagnostic that can quantify *local* model physics error before significant interactions have taken place with (and via) the resolved dynamics.

Slide 22



When predicting uncertainty in climate sensitivity using a perturbed parameter ensemble (of the UK Met Office’s Unified Model HadSM3), Stainforth et al. (2005) found that the model perturbation that led to the largest global warming (up to 12K) in their ensemble was a reduction (by factor 5) in the turbulent entrainment coefficient for convection. The blue dots in the left panel show all the models that included such a perturbation. These perturbed models could not be rejected based on their abilities to simulate present-day climate (they were well inside the present-day climate errors of the CMIP2 models which were ~2.0). This assessment is after each physics perturbation has had time to interact with the global circulation. Further details about the numbers plotted in the figure can be found in the methods section of Stainforth et al. (2005). In brief, RMS error is the square-root of the average, over several variables, of the area-integrated squared climate error of a perturbed model normalised by that of the unperturbed model. Climate sensitivity is the difference between predicted equilibrium global-mean near-surface temperature (with 2x CO<sub>2</sub>) and the global-mean near-surface temperature within their “present-day” control period (with 1x CO<sub>2</sub>). The top right panel shows the initial tendencies associated with the dominant physical processes (and the dynamics) within the ECMWF (unperturbed) model for the Amazon region (based on a model version that was operational in 2005). It can be seen that convective (Con) heating is balanced by dynamic (Dyn) cooling due to ascent and also by radiative (Rad) cooling. The first-guess tendency is simply the sum the individual process tendencies. It can be seen that this total initial tendency is ‘small’ and thus the model physics is ‘reasonable’. When the entrainment parameter is reduced by a factor 5 in the ECMWF model and a new data assimilation / forecast cycle experiment made, it is found (bottom right panel) that the initial tendencies are not so well in balance. The total tendency (red) is equal to (minus) the mean analysis increment and hence the model (physics) appears to be inconsistent with (observations of) the real world. Rodwell and Palmer (2007) argued that this model perturbation was therefore unphysical and could be rejected (or perhaps down-weighted) within a perturbed parameter ensemble. If this result carried over to the UK

Met Office's model, in this particular case, the uncertainty in climate change would be substantially reduced (removal of all blue dots in the left panel). The initial tendency approach is much less computationally expensive than running a coupled model for hundreds of years. This provides justification for pursuing a seamless approach to weather and climate forecasting. See the more recent paper by Sexton et al. (2019).


We can begin to understand physically what is happening in the model with reduced entrainment: with less entrainment, less buoyancy is detrained from a convective plume, which thus rises higher and heats more. Initially, this increased heating is not balanced by increased dynamical cooling since the large-scale dynamics are better constrained by the observations, and respond more slowly. Later in the forecasts, the processes within this perturbed model must also come into balance (when the atmospheric state approaches the climate attractor of the perturbed model). Interestingly, the Amazonian precipitation climate of the perturbed model is actually less than that of the control model – highlighting the issues of interpretation after processes have had time to interact: a key reason for looking at the shortest relevant timescales.

Note that such results may have implications for the permissible range of parameter uncertainties within the model uncertainty parametrization via stochastic perturbations to parameters (SPP).

## Slide 23

Summary

- Tropical waves, teleconnections, and the propagation of errors
  - Important for predictability
  - Can complicate the diagnosis of forecast system deficiencies
- Identifying the root-causes of forecast errors and assessing models
  - Diagnosis at short leadtimes (associated with data assimilation) can localise errors (geographically, process-wise, model versus observation) before errors and uncertainties have had time to propagate and interact
  - Don't need mean error patterns to agree at short-range and long ranges (although sometimes bias patterns do simply grow in magnitude)
- Next lecture: Ensemble aspects, Uncertainty growth, "Classifying and modelling butterflies"

 European Centre for Medium-Range Weather Forecasts Mark J. Roberts 23